Two-dimensional phase transitions studied by thermal He scattering

Klaus Kern, Peter Zeppenfeld, Rudolf David, and George Comsa
Institut für Grenzflächenforschung und Vakuumphysik, Kernforschungsanlage Jülich, Postfach 1913, D-5170 Jülich, West Germany

(Received 23 September 1987; accepted 9 November 1987)

The structure of physisorbed rare-gas layers depends on the interplay between the mutual interaction of the rare-gas atoms and the periodic corrugation of the substrate holding potential. A fascinating variety of structural phases and of mutual phase transformations of these layers adsorbed on graphite and on Pt(111) has been observed. This variety is due to the delicate balance between these interactions. This balance is also the cause for radical changes of salient layer features induced by minute amounts of impurities and defects. High-resolution thermal He scattering appears to be particularly appropriate for an exhaustive investigation of the properties of these layers: simple diffraction patterns (no substrate scattering contribution) including sensitivity for shallow periodic buckling as well as high-resolution (<0.4 meV) energy-loss spectra are the main capabilities which allow for a complete analysis of the structure and dynamics of these layers. The extreme sensitivity for surface defects and impurities, and the absence of any disturbance induced by the He beam are further advantages.

I. INTRODUCTION

The static and dynamic properties of solid surfaces on an atomic length scale are conveniently derived from a scattering experiment. The probe particles can be thermal neutrons, x-ray photons, low-energy electrons, or thermal He atoms. The first two probe particles have the advantage and disadvantage of a weak scattering interaction, allowing the application of the kinematical approximation to extract structural information but making these probe particles basically surface insensitive. In these cases surface sensitivity can be obtained either by using grazing angles of incidence (x rays) or by using substrates with large surface-to-volume ratio like powdered samples (neutrons). On the other hand, electrons and He atoms have stronger scattering interactions which may complicate the structural analysis, but which also ensures an information depth which is confined to a few layers (electrons) or to the outermost surface layer only (He atoms).

It is this exclusive surface sensitivity of thermal atom scattering which makes this method to an outstanding surface probe. This has been recognized more than 60 years ago by Johnson[1]: "These experiments are of interest not only because of their confirmation of the predictions of quantum mechanics, but also because they introduce the possibility of applying atom diffraction to investigations of the atomic constitution of surfaces. A beam of atomic hydrogen, for example, with ordinary thermal velocities, has a range of wavelengths of the right magnitude for this purpose, centering around 1 Å, and the complete absence of penetration of these waves will insure that the effects observed arise entirely from the outermost atomic layer." In spite of this early recognition of the potential provided by thermal atoms to study surfaces, the lack of an appropriate He beam source was the main hurdle in the development of this now very powerful analytical tool. For a long time the Knudsen (effusion) cell has been the only means for producing molecular beams. The Maxwellian effusive beams have low intensity ($I_0 \approx 10^{14}$ particles s^{-1} sr^{-1}) and low monochromaticity ($\Delta v/v = \Delta\lambda/\lambda = 0.95$). Monochromaticity improvement by means of mechanical velocity selectors reduces the already low intensity to a level which in view of the inefficient He detection is unacceptable for a decent analysis. The major breakthrough has been the development of high-pressure nozzle sources. The effect achieved by the invention of these sources is only comparable to that of the laser technology: simultaneous increase of intensity and monochromaticity by several orders of magnitude. Indeed, intensities of 10^{19} particles s^{-1} sr^{-1} and monochromaticities of $\Delta v/v = \Delta\lambda/\lambda \approx 0.01$ are obtained routinely today. Here, we want to discuss the basic features of He-atom scattering with particular emphasis to the study of labile quasi-two-dimensional physisorbed overlayers.

The major characteristics of the He beam as surface analytical tool are connected with the nature of the He–surface interaction potential. At distances not too far from the surface, the He atom is weakly attracted due to dispersion forces. At a closer approach, the electronic densities of the He atom and of the surface atoms overlap, giving rise to a strong repulsion. The classical turning point for thermal He is a few angstroms in front of the outermost surface layer. It is this interaction mechanism which makes the He atom sensitive exclusively to the outermost layer. The low energy of the He atoms and their inert nature ensures that He scattering is a completely nondestructive surface probe. This is particularly important when delicate phases, like physisorbed layers, are investigated. The de Broglie wavelength of thermal He atoms is comparable with the interatomic distances in adsorbed overlayers. Thus from measurements of the angular positions of the diffraction peaks the size and orientation of the two-dimensional (2D) unit cell, i.e., the structure of the outermost layer can be straightforwardly determined. Analysis of the peak intensities yield the potential corrugation, which usually reflects the geometrical arrangement of the atoms within the 2D unit cell.[2]

The energy of thermal He atoms is comparable with the

 0734-2101/88/030639-07$01.00

energies of collective excitations (phonons) in overlayers. Thus, in a scattering experiment the He atom may exchange an appreciable part of its energy with the surface. This energy can be measured in time-of-flight experiments with a resolution ~ 0.3 meV; the resolution can be brought even to ~ 0.1 meV (when using very low beam energies, $\simeq 8$ meV). Thus, surface phonon dispersion curves of rare-gas layers can be mapped out by measuring energy-loss spectra at various momentum transfers in different crystallographic directions. This is a definite advantage of inelastic He scattering over inelastic neutron scattering. (In view of the random orientation of powdered samples, which have to be used in neutron scattering, only average phonon density of states, but not dispersion curves can be obtained.) The range of energy transfer that can be covered by thermal He atoms is limited at the low end by the present maximum resolution of ~ 0.1 meV and at the high end by the nature of the scattering mechanism. The thermal He-beam–surface interaction time being finite, the upper limit for the observable phonon modes is ~ 40 meV. So far only modes with a component perpendicular to the surface have been clearly detected; this seems to be less a fundamental, but rather a technical problem.

Besides the inelastic component, always a certain amount of elastically scattered He atoms is found also in between the coherent diffraction peaks. We will refer to this scattering as diffuse elastic scattering. This diffuse intensity is attributed to scattering from defects and impurities. Accordingly, this diffuse elastic scattering provides valuable information on the degree and nature of surface disorder. It can be used, for example, to study the growth of thin films[3] or to deduce information on the size, nature, and orientation of surface defects.[4] Very recently the peak width analysis of the diffuse elastic component has also been used to study the diffusive motion of surface atoms.[5]

Another remarkable way to use He scattering for the study of adsorbed layers is based on the large total cross section Σ for diffuse He scattering of isolated adsorbates (e.g., in the case of adsorbed Xe, $\Sigma_{Xe}^{He} \approx 110$ Å^2 for $E_{He} = 18$ meV). This large cross section is attributed to the long-range attractive interaction between adatom and the incident He atom, which causes He atoms to be scattered out of the coherent beams. The remarkable size of the cross section allows the extraction of important information concerning the lateral distribution of adsorbates, mutual interactions between adsorbates, dilute-condensed phase transitions in 2D, adatom mobilities, etc.,[6] simply by monitoring the attenuation of one of the coherently scattered beams, in particular of the specular beam. This technique also allows the detection of impurities (including hydrogen!) in the per mill range, a level hardly attainable with almost all other methods.

II. EXPERIMENTAL

In Fig. 1 we show a schematic sketch of the high-resolution He-scattering spectrometer used in the authors' laboratory.[7] The scattering geometry is fixed with $\vartheta_i + \vartheta_f = 90°$, where ϑ_i and ϑ_f are incident and outgoing angles, respectively. The vacuum system consists of four main units: the three-chamber nozzle beam generator, the scattering chamber (with sample holder, low-energy electron diffraction, cylindrical mirror analyzer–Auger, and ion gun facilities), the pseudorandom chopper chamber, and the three-chamber detector unit. The scattering chamber has a base pressure in the low 10^{-11} mbar range which rises to $\sim 10^{-9}$ mbar (He partial pressure) during He-beam operation. The extensive differential pumping [turbomolecular pumps (TMP's)] serves to reduce the He partial base pressure in the detector chamber to 10^{-15}–10^{-16} mbar. As detector we use a commerical Extranuclear mass spectrometer with electron bombardment ionizer; the residual He pressure in the detector chamber results in a count rate of ~ 40 counts/s at 5-mA emission current. This figure has to be compared with 10^5 counts/s, representing the signal of the first-order He diffraction beam ($E_{He} = 18$ meV) from a Kr monolayer adsorbed on Pt(111) at 25 K.

In most experiments a 18-meV He beam, produced by cooling the nozzle with liquid nitrogen, is used. The particle flux impinging on the target is $\sim 2 \times 10^{19}$ He atoms s^{-1} sr^{-1} with a velocity spread $\Delta v/v = 0.007$ (He stagnation pres-

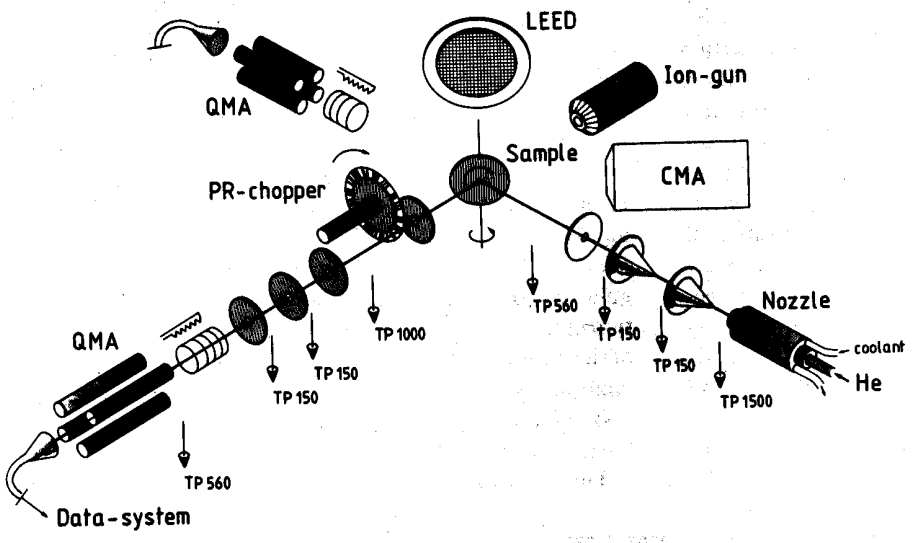

FIG. 1. Schematic view of the high-resolution He surface scattering spectrometer.

sure: 150 bar). The beam divergence as well as the acceptance angle of the detector are 0.2°. Accordingly, the overall momentum resolution (FWHM) of the apparatus is ~ 0.01 Å^{-1}, corresponding to a transfer width for the higher-order peaks around 200–300 Å. Information on correlation lengths up to 1000 Å can be inferred by instrumental response function deconvolution of diffraction peaks monitored with appropriate statistics.

The energy distribution of the scattered He atoms is obtained by a cross correlation analysis of the time-of-flight (TOF) spectra of the He atoms upon passing a pseudorandom chopper.[7] At a flight path of 790 mm the overall resolution of the spectrometer for a 18-meV beam with $\Delta v/v = 0.007$ is 0.4 meV.

All experiments reported here are performed with a Pt(111) crystal surface as substrate. The crystal is mounted on a manipulator which allows independent polar and azimuthal rotation as well as tilting. The temperature can be regulated between 25 and 1800 K by means of liquid-He cooling and/or electron bombardment heating.

The temperature of the crystal is controlled by a Chromel–Alumel thermocouple calibrated *in situ* by Xe vapor-pressure isotherms monitored with surface phonon spectroscopy.[7,8] The Pt crystal is cleaned by repeated cycles of argon and xenon ion bombardment and annealing to 1200 K. The defect density of the clean Pt surface is $< 10^{-3}$ (average terrace width 2000–3000 Å) as probed with elastic He scattering.

III. ISLANDING AND THE LATERAL ADATOM INTERACTION

Structural phase transitions in adsorbed layers are governed by the delicate balance between the lateral adatom interaction and the corrugation of the adatom–substrate holding potential. Due to the presence of the substrate, the lateral interaction potential is a complicated composition of direct and indirect, substrate mediated terms. Thus, it is worthwhile to extract lateral adatom energies from simple experiments.

It has been shown recently by Poelsema *et al.*[9] that the 2D gas↔2D solid + 2D gas-phase transition, i.e., 2D islanding, can be studied in an elegant way by means of specular He scattering. The specular He peak height scattered from a crystal surface in the presence of a 2D lattice gas of adparticles is an unequivocal, extremely sensitive function of the adparticle coverage, according to

$$I/I_0 \simeq (1-\theta)^{n_s \Sigma}, \tag{1}$$

with θ the coverage, Σ the scattering cross section for diffuse scattering per adatom, and n_s the density of adsorption sites. However, when islanding starts, i.e., at the 2D gas→2D solid + 2D gas transition, the subsequent attenuation of the specular intensity versus coverage is determined by the much smaller geometrical cross section A of the adatoms in the 2D condensed phase:

$$I/I_c \simeq 1 - A n_s(\theta - \theta_c), \tag{2}$$

with I_c being the specular intensity at the critical coverage θ_c, where condensation sets in. In Fig. 2 we show the specular intensity reflected from a Pt(111) surface at 54 K as a function of Kr exposure.

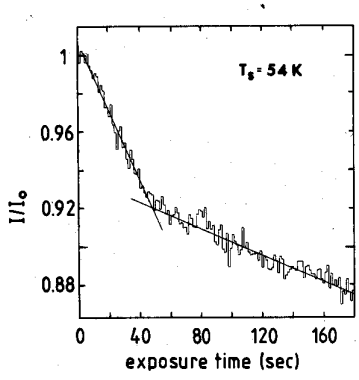

FIG. 2. Specularly reflected He-beam intensity from a Pt(111) surface at $T_s = 54$ K upon exposure of Kr ($p_{Kr} = 2.1 \times 10^{-9}$ mbar).

From the initial slope of the curve, which is governed by Eq. (1), the value of the scattering cross section Σ_{He}^{Kr} is directly obtained provided the sticking probability of Kr is known. In Table I the inferred scattering cross sections for diffuse scattering of 18-meV He atoms from Xe, Kr, and Ar on Pt(111) are presented.

The sudden slope change in Fig. 2 obviously marks the onset of islanding. The corresponding coverage θ_c corresponds to the 2D vapor pressure of Kr on Pt(111). From measurements of θ_c at different temperatures, the 2D latent heat of vaporization is obtained under the assumption that the 2D gas is nearly perfect.[9]

In Table II the 2D latent heats of vaporization obtained in this way for Xe, Kr, and Ar on Pt(111) are listed. They represent actually the lateral interaction energy between the adlayer atoms.

TABLE I. Total scattering cross section for He scattering (18.3 meV) from adsorbed rare gases on Pt(111).

	Xe	Kr	Ar
Σ(Å^2)	110	70	52

IV. ROTATIONAL EPITAXY OF MONOLAYERS

The lateral interaction energy of Xe on Pt(111) is 43 meV. This number has to be compared with the lateral corrugation of the holding potential, the average value of which has been measured in a recent investigation[10] to be ~ 30 meV. It is the competition between these two nearly equal interaction strengths which gives rise to a large variety of structural phases and phase transitions. Indeed, as a function of temperature and coverage, Xe monolayers on Pt(111) exhibit a wealth of structures ranging from a commensurate $(\sqrt{3}\times\sqrt{3})R$ 30° hexagonal phase, over striped and hexagonal

TABLE II. Lateral interaction energies for rare gases adsorbed on Pt(111).

	Xe	Kr	Ar
ϵ_l(meV)	43	26	17

R 30° incommensurate ones, and reaching finally at monolayer saturation a hexagonal R 30° ± 3.3° rotated phase.[11–13]

For small misfits, the incommensurate phases have the same orientation as the commensurate structure, 30° rotated with respect to the substrate. In this range of incommensurabilities, the misfit strain of the incommensurate layer is minimized by the formation of misfit dislocations, i.e., so-called domain walls. By the formation of domain walls, only longitudinal strains in the monolayer are affected. In two-dimensional incommensurate overlayers, however, longitudinal as well as transverse strains are present. Since transverse strains have lower energy than longitudinal strains in a 2D layer (transverse phonons are softer than longitudinal ones), the interconversion of these strains may minimize the total energy of the overlayer by rotating the adlayer out of the symmetry axes of the substrate. Indeed, Novaco and McTague[14] have shown that for monolayers far from commensurability these rotations are energetically favorable. Novaco and McTague also showed that this rotational epitaxy involves mass density waves (MDW) [also known as static distortion waves (SDW)], i.e., there exists a periodic deviation of the position of monolayer atoms from their regular lattice sites. Indeed, it is the combination of rotation and small displacive distortions of the adatom net which allows the adlayer to minimize its total energy in the potential relief of the substrate. In a diffraction experiment, these mass density waves should give rise to satellite peaks.

Fuselier *et al.*[15] have introduced an alternative concept to explain the adlayer rotation: the "coincident site lattice." They pointed out that energetically more favorable orientations are obtained for rotated high-order commensurate structures. The larger the fraction of adatoms located in high-symmetry, energetically favorable sites, the larger the energy gain and the more effective the rotated layer is locked. It turns out that the predictions of the coincident site lattice concept for the rotation angle versus misfit agrees well with the Novaco–McTague predictions.

The Novaco–McTague rotational epitaxy has been observed in numerous adsorbate systems including Ar, Ne, and Kr on graphite, Na/Ru(100), K/Cu(100), and K/Pt(111) (for references see Ref. 13). It has also been observed for Xe monolayers on Pt(111) at large incommensurabilities. When increasing the misfit above 7.2% the hexagonal incommensurate (HI) phase transforms by a continuous transition into a hexagonal incommensurate rotated (HIR) phase.[13]

Figure 3 is a plot of the rotation angle φ as a function of the average misfit during the HI–HIR transitions; the black dots are the measured data. The dashed line is the Novaco–McTague linear response theory for a Cauchy solid. Shiba[16] noted that with increasing misfit a crossover from the domain wall regime (small incommensurabilities) to the modulation regime (large incommensurabilities) should occur, and that there should be a finite misfit for the onset of rotation. His curve for a Cauchy solid is also drawn in Fig. 3 (dashed–dotted) for the value of his parameter l which causes the HI–HIR transition to occur at the experimental critical misfit of 7.2% (here $l \simeq 10$). Shiba's theory gives a qualitative account of the overall variation of rotation angle

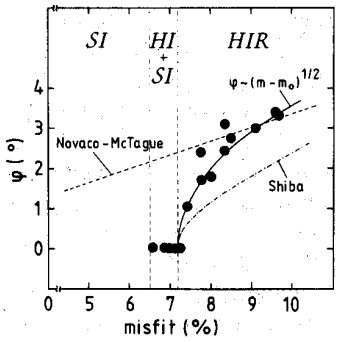

FIG. 3. Rotation angle φ of Xe monolayers on Pt(111) vs misfit (see text).

versus misfit but no quantitative acount. Actually, the data are fitted well by a power law of the form $\varphi \sim (m - m_0)^{1/2}$ with $m_0 = 0.072$, which is shown as a solid line in Fig. 3. A similar power law behavior has been observed for the rotation angle of Kr layers on graphite[17] and in Cs intercalated graphite.[18]

It is worthwhile to address here the question concerning the physics behind the rotational epitaxy; mass density waves[14] or high-order commensurability?[15] In a He diffraction study of rotated Xe monolayers on Pt(111) we have, indeed, observed satellite peaks and assigned them to a higher-order commensurate superstructure.[3] However, Gordon[19] pointed out that these satellites could be due to the MDW. Here, we will show that both MDW as well as commensurate buckling satellites are present in the rotated Xe monolayers on Pt(111). The distinction between the two types of satellites is straightforward. As pointed out by Gordon, the MDW satellites should be subject to the following relation:

$$Q \simeq (8\pi/d^{R}_{Xe})(m/\sqrt{3})(1 + m/8), \tag{3}$$

where Q is the wavevector of the satellites, m the misfit, and d^{R}_{Xe} the lattice constant of the rotated Xe layer. For not too large misfits, this MDW satellite should appear in the same direction as the principal reciprocal lattice vector of the Xe layer, i.e., in the $\bar{\Gamma}\bar{M}_{Xe}$ direction. On the other hand, the commensurate buckling, according to its peculiar structure (Fig. 3, Ref. 3) should have its maximum amplitude in the $\bar{\Gamma}\bar{K}_{Xe}$ direction. Moreover, these commensurate buckling satellites should only be present at the particular coverage where the high-order commensurability becomes favorable, in the present case at monolayer completion ($m = 9.6\%$) (see also Ref. 20), whereas the MDW satellites should be present in the entire misfit range where the Xe layer is rotated (7.2%–9.6%).

In Fig. 4(a) we show polar He diffraction scans in the vicinity of the specular beam, with the scattering plane oriented along the $\bar{\Gamma}\bar{M}_{Xe}$ direction, for rotated Xe layers of misfit 8.3% and 9.5%, respectively. In both scans satellite peaks are present. The dispersion of these peaks is shown in Fig. 4(b), and compared with Gordon's prediction for the MDW given above. The data follow qualitatively the predicted dependency; the agreement becomes quantitative at misfits $\gtrsim 8\%$. The reason for the better agreement at large misfits is due to the fact that Gordons analysis of the MDW (similar to Novaco–MacTague's model calculations) have been performed in the linear response approximation of the

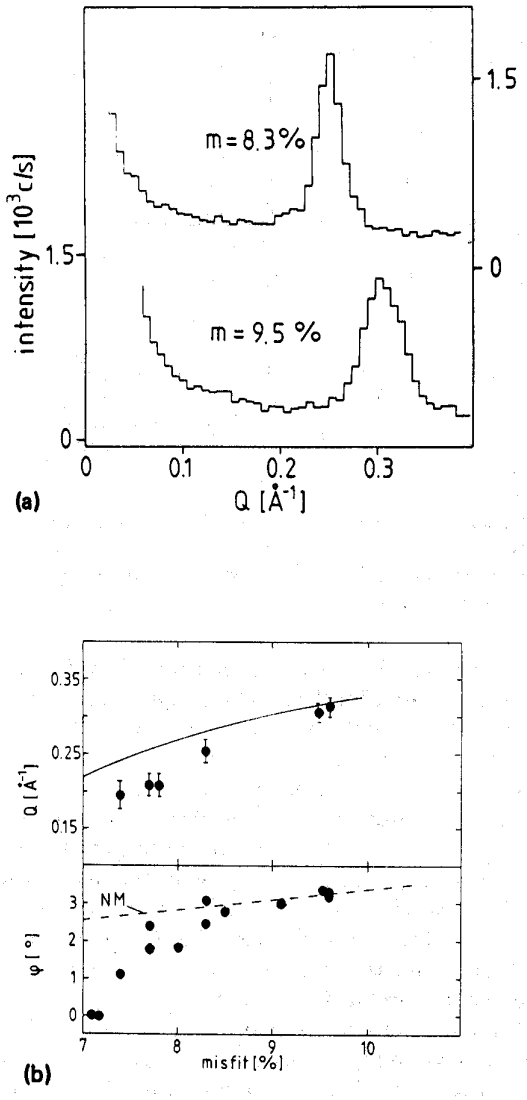

FIG. 4. (a) Polar He diffraction scans of rotated Xe monolayers on Pt(111) taken along the $\bar{\Gamma}\bar{M}_{Xe}$ azimuth at misfits 8.3% and 9.5%. (b) Dispersion of the mass density wave satellites with misfit m. The solid line is Gordon's relation.

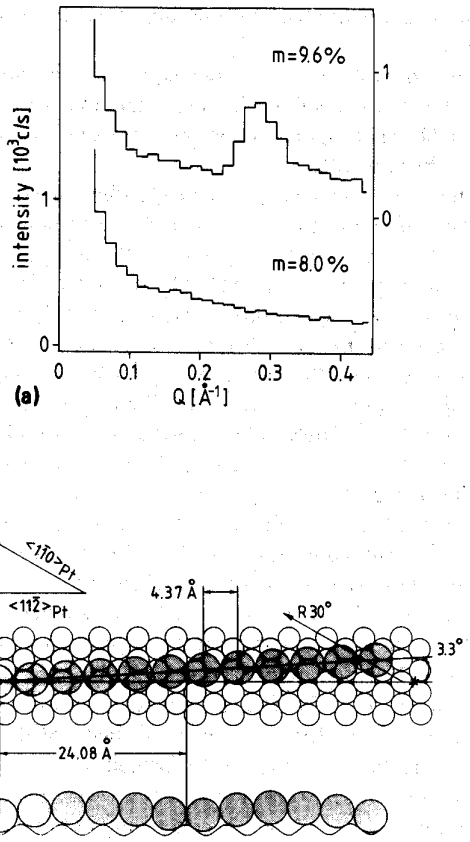

FIG. 5. (a) Polar He diffraction scans of rotated Xe monolayers on Pt(111) taken along the $\bar{\Gamma}\bar{K}_{Xe}$ azimuth as misfits 8% and 9.6%. (b) Upper and side view of a 3.3° rotated domain at the $m = 9.6\%$ misfit.

adsorbate–substrate interaction. As discussed in connection with Fig. 3 above, this approximation is only justified at larger misfits. The measured intensities of the MDW satellites vary between 10^{-2} and 10^{-1} of the strongest Xe layer diffraction peak at small and at large misfits, respectively. These intensities can be correlated with the amplitudes of the MDW. By means of Eqs. (6)–(8) in Ref. 19 and by using realistic values for the Xe/Pt(111) potential MDW amplitudes of the order 0.1 Å are obtained.

In Fig. 5(a) we show scans like in Fig. 4(a) but now measured in the $\bar{\Gamma}\bar{K}_{Xe}$ direction for rotated Xe layers of misfits 8% and 9.6%. At variance with the scans in the $\bar{\Gamma}\bar{M}_{Xe}$ direction [Fig. 4(a)], a satellite peak is observed only for the complete Xe monolayer ($m = 9.6\%$). The location of this satellite peak at $Q = 0.28$ Å^{-1} corresponds to a buckling period of 23 Å and can be ascribed to a high-order commensurate structure shown in Fig. 5(b) and described in detail in Ref. 3. Being present only at a particular misfit this peak does not originate from a MDW. Thus, only at monolayer completion ($m = 9.6\%$) the rotated Xe layer locks in the substrate, i.e., is a high-order commensurate phase.

Thus, the present answer to the question just addressed seems to be that both mass density waves and high-order commensurability may be involved in rotational epitaxy.

V. DEFECTS AND IMPURITIES

Almost all theoretical studies of 2D adsorbed layers deal with perfect substrates, i.e., strictly periodic arrangements of surface atoms extending over infinite distances. In experiment, however, this situation is hardly met. Indeed, unavoidable slight misorientations of the substrate plane with respect to the low-index planes during crystal surface preparation result in a finite step density. Today's best prepared low-index metal surfaces have step densities of ~0.1%, corresponding to average domain sizes of perfect coherence of ~2000–3000 Å. In addition, even under the most careful experimental ultrahigh vacuum conditions (base pressure in the low 10^{-11} mbar range), small amounts of adsorbing impurities (H_2, CO, etc.) cannot be completely avoided.

Recently, several authors[21,22] have explored theoretically the extent to which traces of impurities may influence two-dimensional phase transitions, in particular the commensurate–incommensurate transition. Marked deviations in the

critical behavior induced by the impurities have been predicted.

We readdress here the part played by steps in the condensation of 2D rare-gas films, in particular concerning the orientation of the hexagonal incommensurate adlayers with respect to the substrate.

We have shown recently[23] that depending on the presence or absence of minute amounts ($\sim 0.1\%$) of preadsorbed gases a Kr adlayer may be aligned ($R\,0°$) or rotated by 30° ($R\,30°$) with respect to the Pt(111) substrate, respectively. We have been able to demonstrate in a direct experiment that when the Kr atoms are allowed to nucleate at the residual $\sim 0.1\%$ step sites (the binding energy at step sites is $\sim 25\%$ larger than at terrace sites[24]) the $R\,30°$ orientation is obtained; on the contrary, when the step sites are blocked by preadsorbed CO or H the growing Kr layer is aligned ($R\,0°$) with the substrate.

In this context the following comments are in order. The very high-purity conditions sought in 2D rare-gas layer experiments impose that the adlayer grows in the presence of relatively low 3D rare-gas pressure (usually well below 10^{-6} mbar), i.e., at surface temperatures T_s substantially lower than the 2D critical temperature T_c^{2D}. In order to get an ordered layer, T_s is chosen high enough to ensure a sufficient mobility of the adatoms; however, T_s being still far below T_c^{2D}, the nucleated islands once formed may impose their original orientation to the subsequent growing process, even if the latter were to prefer (energetically) another orientation: it is indeed, improbable that, at $T_s \ll T_c$, the orientation of an already established nucleated island can be radically changed by the "energetical needs" of the subsequently adsorbing atoms. Accordingly, the variety of true equilibrium structures and orientations, due to the balance between intralayer and adlayer–substrate forces, is further increased by phases in which at least the orientation is determined by kinetic (nucleation and growth) processes.

At variance with Kr/Pt(111), the orientation of the Xe islands on the same surface is always $R\,30°$ regardless of the initial step-site condition, free or blocked. The reason might be that accidentally the orientation of Xe islands is the same whether the nucleation takes place at step sites or not; i.e., the orientation of Xe is always "a true equilibrium orientation."

The case of Ar/Pt(111) presented here is in principle similar to Kr/Pt(111); $R\,30°$ and $R\,0°$ orientations of the hexagonal incommensurate Ar layer are observed depending on the step-site condition. However, the actual orientation of the Ar layer appears to be exactly opposite to the Kr case: free and blocked step sites result in the $R\,0°$ and $R\,30°$ orientations of the Ar layer, respectively.

In Fig. 6(a) a polar He diffraction scan from a 0.3-monolayer (ML) Ar film deposited on the *clean* Pt(111) substrate taken along the $\bar{\Gamma}\bar{M}_{Pt}$ azimuth of the Pt(111) substrate is shown. The $(1,1)_{Pt}$ as well as the $(1,1)_{Ar}$ and $(2,2)_{Ar}$ diffraction peaks are obvious, indicating that the incommensurate hexagonal Ar layer is aligned ($R\,0°$) with the Pt(111). In Fig. 6(b) we again show a polar plot of a 0.3-ML Ar film but deposited on a Pt(111) surface with a precoverage of 0.2% CO taken along the $\bar{\Gamma}\bar{K}_{Pt}$ azimuth. The

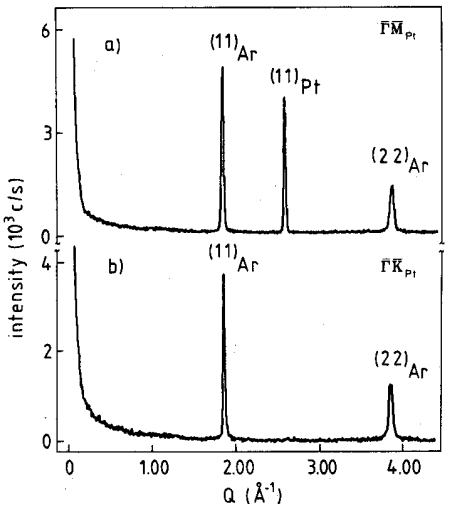

FIG. 6. Polar He diffraction scans monitored in the indicated azimuths from 0.3-ML Ar layers on Pt(111), (a) adsorbed on the clean surface, no precoverage and (b) adsorbed on a surface with a CO precoverage of $\sim 0.2\%$ concentrated on step sites.

$(1,1)_{Ar}$ and $(2,2)_{Ar}$ diffraction peaks are now in the $\bar{\Gamma}\bar{K}_{Pt}$ azimuth indicative for the $R\,30°$ orientation of the Ar layer. [In the $\bar{\Gamma}\bar{M}_{Pt}$ azimuth only the much smaller $(1,2)_{Ar}$ peak is present beside the $(1,1)_{Pt}$ one.] The CO has been deposited at a surface temperature of 200 K where it is fully mobile.[25] As shown by Poelsema *et al.*[25] at this temperature the CO molecules migrate and are eventually bound at step sites, where they remain upon cooling. Since the step density for the crystal used here is $\sim 0.1\%$, the step sites are completely filled by CO before adsorbing Ar. The CO molecules block the step sites and the argon nucleates on the terraces resulting in the $R\,30°$-rotated orientation.

This interpretation is supported by depositing the same 0.2% CO precoverage but at surface temperatures below 150 K. At these low temperatures, the adsorbed CO is immobile, i.e., the molecules stay randomly distributed over terrace and step sites with densities roughly equal to the overall coverage. When adsorbing Ar on a CO-precovered surface prepared in this way, the $(1,1)_{Ar}$ and $(2,2)_{Ar}$ diffraction spots still appear in the $\bar{\Gamma}\bar{M}_{Pt}$ azimuth, as in Fig. 6(a), i.e., randomly distributed CO has no influence on the Ar-layer orientation, which is still $R\,0°$.

These results demonstrate the decisive role steps can have in condensation of rare-gas layers on surfaces. For the puzzling difference in the behavior of Kr and Ar on the same Pt(111) surface we have no explanation so far.

VI. CONCLUSION

We have given here a few examples of how the advantages inherent to thermal He atoms as a surface probe can be used to study physisorbed rare-gas layers. Of course, the application of the method is neither restricted to rare gases nor to physisorption. Chemisorbed layers and clean surfaces are a matter of current experimental studies as well. In particular, by using high-resolution He scattering in various modes—diffraction, coherent inelastic (see for instance Refs. 26 and 27), and diffuse elastic scattering—this probe allows a non-

destructive, nearly exhaustive characterization of the thermodynamics, structure, and dynamics of adsorbate covered as well as of clean, arbitrary monocrystalline surfaces.

[1]T. H. Johnson, Phys. Rev. **37**, 847 (1931).
[2]T. Engel and K. H. Rieder, *Springer Tracts in Modern Physics* (Springer, Berlin, 1982), Vol. 91.
[3]K. Kern, R. David, R. L. Palmer, and G. Comsa, Phys. Rev. Lett. **56**, 2823 (1986).
[4]A. M. Lahee, J. R. Manson, J. P. Toennies, and Ch. Wöll, Phys. Rev. Lett. **57**, 471 (1986).
[5]J. W. Frenken J. P. Toennies, and Ch. Wöll (to be published).
[6]G. Comsa and B. Poelsema, Appl. Phys. A **38**, 153 (1985).
[7]R. David, K. Kern, P. Zeppenfeld, and G. Comsa, Rev. Sci. Instrum. **57**, 2771 (1986).
[8]K. Kern, R. David, R. L. Palmer, and G. Comsa, Surf. Sci. **175**, L669 (1986).
[9]B. Poelsema, L. K. Verheij, and G. Comsa, Phys. Rev. Lett. **51**, 2410 (1983).
[10]K. Kern, P. Zeppenfeld, R. David, and G. Comsa, J. Electron Spectrosc. **44**, 215 (1987).
[11]K. Kern, R. David, R. L. Palmer, and G. Comsa, Phys. Rev. Lett. **56**, 620 (1986).
[12]K. Kern, R. David, P. Zeppenfeld, R. L. Palmer, and G. Comsa, Solid State Commun. **62**, 361 (1987).
[13]K. Kern, Phys. Rev. B **35**, 8265 (1987).
[14]A. D. Novaco and J. P. McTague, Phys. Rev. B **19**, 5299 (1979).
[15]C. R. Fuselier, J. C. Raich, and N. S. Gillis, Surf. Sci. **92**, 667 (1980).
[16]H. Shiba, J. Phys. Soc. Jpn. **48**, 211 (1980).
[17]K. L. D'Amico, D. E. Moncton, E. D. Specht, R. J. Brigenau, S. E. Nagler, and P. M. Horn, Phys. Rev. Lett. **53**, 2250 (1984).
[18]T. Clarke, N. Caswell, and P. M. Horn, Phys. Rev. Let. **43**, 2018 (1979).
[19]M. B. Gordon, Phys. Rev. Lett. **57**, 2094 (1986).
[20]K. Kern, P. Zeppenfeld, R. David, and G. Comsa, Phys. Rev. Lett. **59**, 79 (1987).
[21]J. Villain, J. Phys. (Paris) Lett. **43**, 1551 (1982).
[22]M. Kardar and D. R. Nelson, Phys. Rev. Lett. **55**, 1157 (1985).
[23]K. Kern, P. Zeppenfeld, R. David, and G. Comsa, Phys. Rev. Lett. **57**, 3187 (1986).
[24]R. Miranda, S. Daiser, K. Wandelt, and G. Ertl, Surf. Sci. **131**, 61 (1983).
[25]B. Poelsema, L. K. Verheij, and G. Comsa, Phys. Rev. Lett. **49**, 1731 (1982).
[26]J. P. Toennies, J. Vac. Sci. Technol. A **2**, 1055 (1984).
[27]K. Kern, P. Zeppenfeld, R. David, and G. Comsa, Phys. Rev. B **35**, 886 (1987).